Model intercomparison for the AWAKEN King Plains wind farm in idealized unstable and stable conditions

Myra Blaylock[1], Kenneth Brown[2], Bruno Carmo[7], Lawrence Cheung[1], Nathaniel deVelder[2], Nicholas Hamilton[4], Thomas Herges[2], Daniel Houck[2], Alan Hsieh[2], Colleen Kaul[3], David Maniaci[2], Pedro Peixoto[6], William Radünz[5*], Raj Rai[3], Alex Rybchuk[4], Philip Sakievich[2], Ryan Scott[4], Regis Thedin[4]

[1]Sandia National Laboratories, Livermore CA 94550, USA
[2]Sandia National Laboratories, Albuquerque, NM 87185, USA
[3]Pacific Northwest National Laboratories, Richland WA 99354, USA
[4]National Renewable Energy Laboratory, Golden, CO 80401, USA
[5]Centre of Dynamics and Fluids, Polytechnic School, University of São Paulo, Brazil
[6]Department of Applied Mathematics, University of São Paulo, Brazil
[7]Department of Mechanical Engineering, Polytechnic School, University of São Paulo, Brazil

mlblayl@sandia.gov, kbrown1@sandia.gov, bruno.carmo@usp.br, lcheung@sandia.gov, ndeveld@sandia.gov, Nicholas.Hamilton@nrel.gov, therges@sandia.gov, ahsieh@sandia.gov, colleen.kaul@pnnl.gov, dcmania@sandia.gov, ppeixoto@usp.br, wradunz@usp.br, raj.rai@pnnl.gov, Alex.Rybchuk@nrel.gov, Ryan.Scott@nrel.gov, Regis.Thedin@nrel.gov

RESUMO

Uma série de simulações numéricas de um parque eólico, utilizando diferentes fidelidades de modelos e para diferentes condições de estabilidade atmosférica, foram realizadas como parte do American WAKE Experiment (AWAKEN). As simulações incluem o uso do modelo de esteira FLORIS, algumas simulações de microescala com os modelos AMR-Wind e Nalu-Wind, assim como simulações idealizadas com WRF-LES-GAD, com e sem terreno. As simulações de grandes escalas (LES) focaram em seções do parque eólico King Plains do AWAKEN. Resultados dessa comparação ilustram as interações entre um parque eólico com estruturas de grande escala da camada limite atmosférica (CLA) no escoamento, bem como a extensão do efeito de esteira do parque à jusante. Diferenças na variabilidade no campo do vento, turbulência e recuperação da esteira são distinguíveis entre os casos instável e estável. Entretanto, ambas fontes esperadas e inesperadas de variabilidade inter-modelo levaram a diferenças de vento, turbulência e esteira.

Palavras-chave:
Modelagem numérica e simulação; Intercomparação de modelos; AWAKEN; parque eólico; LES

ABSTRACT

A series of numerical simulations of a wind farm, using different model fidelities and for different atmospheric stability conditions, were performed as a part of the American WAKE ExperimeNt (AWAKEN). The simulations included using FLORIS wake models, a number of microscale AMR-Wind and Nalu-Wind runs, as well as idealized WRF-LES-GAD runs with and without terrain. The LES computations focused on sections of the AWAKEN King Plains wind farm. Results of this comparison illustrate the interactions of a wind farm with large-scale ABL structures in the flow, as well as the extent of downstream wake penetration in the flow. Differences in the wind flow field variability, turbulence, and wake recovery are distinguishable between the unstable and stable cases. However, both expected and unexpected sources of variability across models led to differences in wind, turbulence, and wakes.

Keywords:
Numerical modeling and simulation; Model intercomparison; AWAKEN; wind farm; LES

1. INTRODUCTION

One of the most effective approaches to accelerate the large-scale deployment of wind energy is to lower the levelized cost of energy (LCoE) associated with projects. That can be achieved by improved understanding of uncertainties related to the expected project performance in the long-term. A large share of these uncertainties is related to the numerical models used in conjunction with on-site mast or lidar observations to represent the wind resource and turbine wakes in and around wind farms. These range in fidelity from simple and computationally fast engineering or analytical models to more complex and computationally expensive multiscale large-eddy simulation (LES) models.

Engineering models such as the FLOw Redirection and Induction in Steady State (FLORIS) framework [1] need to be fast because they are intended for wind farm layout optimization, which requires thousands of runs or more. The LES-based models, such as AMR-Wind [2], Nalu-Wind [2, 3] and WRF-LES [4], tend to require the usage of high-performance computing (HPC) facilities and thus their application is mostly intended for scientific research and final-stage wind farm project analysis, although advances in computation enabled by graphical processing units (GPUs) may soon enhance their scope of applications [5]. The higher cost is justified by their ability to represent a wide range of scales of turbulent motion, different atmospheric stability regimes, gravity waves, wind farm wake development [6], merging and superposition, blockage [7] and even topographic effects in some cases. Therefore, this higher physical fidelity is important to inform, develop and tune engineering models.

The validation of higher fidelity LES models requires dedicated field measurements of the atmospheric boundary layer (ABL) winds, turbulence and stability, as well as real performance data of the wind farms operating in that environment. Wind-energy field experiments are not new [8–11], but up until recently no past experiment combined high spatio-temporal resolution measurements of ABL structure, winds, turbulence and wakes in and around real wind farms, and performance data. To fill this scientific gap, the US Department of Energy (DoE) and the National Laboratories organized the ongoing American WAKe Experiment (AWAKEN) project, a collaborative effort between government, national laboratories, academia, and industry [12]. The main goal is to understand the environmental factors that influence real wind farm performance in simple terrain, such as wakes, blockage, and turbulence regimes using field observations, and to develop numerical models capable of representing those features. The selected study area is a cluster of wind farms located in the Southern Great Plains (SGP) in Oklahoma, owing to the interesting meteorological processes that occur there (such as nocturnal low-level jets – LLJs) and the somewhat gentle slopes of the terrain.

The goal of this study is to perform a modeling intercomparison benchmark in idealized unstable and stable stability conditions to investigate how differences in features such as actuator disk model (ADM) type, terrain, atmospheric stability, among other model subtleties influence the simulated wind, turbulence, wakes and farm performance. A portion of the King Plains wind farm, part of the AWAKEN experiment, is simulated using the LES-based models AMR-Wind, Nalu-Wind and WRF-LES, as well as the FLORIS engineering model. This is intended to pave the way to future studies that include observations and real wind farm performance data collected in the AWAKEN project.

2. DATA AND METHODS

2.1. The AWAKEN project King Plains wind farm and idealized inflow conditions

The AWAKEN field experiment takes place in the Southern Great Plains (SGP) in Oklahoma, U.S [12]. The King Plains wind farm is shown overlayed to the digital elevation model in Fig. 1. Horizontal variations in terrain height are gentle within and around the 88 GE2.8-127 turbines that integrate King Plains. In the subsequent modeling setups, either the whole wind farm or the eastern portion of it will be simulated.

The conditions for the numerical simulations are derived from measurements at the nearby Atmospheric Radiation Measurement (ARM) Southern Great Plains facility. Table 1 shows the data taken at the ARM Central Facility (site C1) and includes wind speed, turbulence, and shear information collected from Jan. 2015 to Nov. 2020. In all cases, the primary wind direction was 175±10◦. Data corresponding to unstable, near-neutral, and stable conditions were available, although the current study focuses on simulations of the unstable and stable atmospheric boundary layer (ABL).

2.2. Numerical models

A summary of the different simulations performed as a part of this milestone is provided in Table 2. The major focus for many of the simulations was the eastern section of the King Plains wind farm, which corresponds to the location of several planned AWAKEN lidar and turbine instrumentation sites. The unstable case additionally employs the WRF-LES-GAD and FLORIS-Gaussian models, in comparison to the stable case.

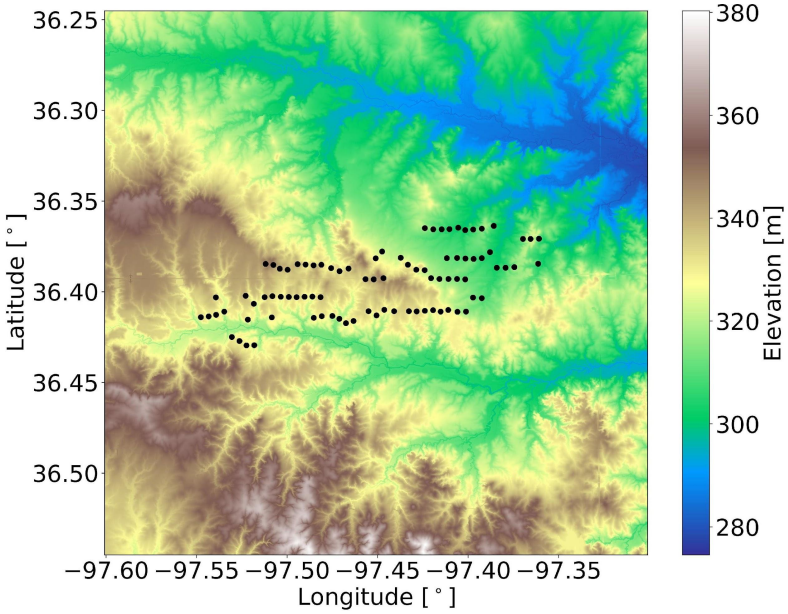

Fig. 1. The eighty-eight turbines that compose the King Plains wind farm (black dots) overlayed to the digital elevation model of the region.

Table 1
Atmospheric boundary layer parameter values for each study case.

Parameter	Unstable	Stable
Wind speed at 91 m (U_{91}) [m/s]	9.0	10.1
Wind shear exponent (α)	0.09	0.32
Air potential temperature at 3 m (θ_3) [K]	305.8	302.3
Friction velocity ($u_\star$) [m/s]	0.49	0.32
Turbulence intensity at 60 m (TI_{60}) [%]	18	9.6

Table 2
Suite of numerical models employed for each study case.

Unstable	Stable
AMR-Wind	AMR-Wind
Nalu-WindNalu-Wind	
WRF-LES-GADFLORIS-TurbOPark	
FLORIS-TurbOPark FLORIS-Gaussian	

2.2.1. FLORIS

Wind plant simulations were performed with the FLOw Redirection and Induction in Steady State (FLORIS) framework, version 3.1. Turbine models were created using WISDEM/WEIS and manually adjusted to match observed power from SCADA where possible. The TurbOPark model [13] was selected for simulations of the complete AWAKEN system based on comparisons between the available models in FLORIS and measured turbine power. This model was designed to capture far wake expansions and has shown good agreement with measured plant performance in offshore settings. Model parameter tuning was achieved by minimizing the difference between FLORIS frequency-weighted mean power estimates and the frequency-weighted mean power measured at King Plains for each atmospheric condition. Optimal agreement between data sets was realized by increasing FLORIS turbulence intensity by a constant 2.5% and setting the wake expansion parameter, A, to 0.2. Hub-height flow fields were obtained for King Plains with the Gauss-Curl Hybrid (GCH) model [14]. The GCH model is designed to capture wake dynamics on the order of typical turbine spacing and includes the effects of secondary steering within the plant.

2.2.2. AMR-Wind

AMR-Wind [2] solves the incompressible Navier-Stokes equations with variable density and viscosity. Additionally, scalar transport equations can be solved, such as potential temperature or turbulent kinetic energy. The discretization in AMR-Wind is based on the approximate projection method used in IAMR [15] and *incflo* [16]. It is a semi-staggered scheme where the velocity and scalar variables are located at cell centers and pressure is located at nodes. Pressure is also staggered in time so that pressure and the pressure gradient are at time $n + 1/2$. The time discretization is handled with a Crank Nicholson approach, and the advection term is handled explicitly using an upwind finite-volume method using the WENO-Z algorithm [17]. The diffusion terms can be handled explicitly, semi-implicitly, or implicitly and are spatially discretized using a second-order central difference formula. For the simulations in this paper, we used an implicit scheme for the viscous terms, as the variable viscosity from the eddy viscosity may cause time step restrictions. After the scalar equations and the momentum equations are advanced in time, a nodal projection is used to approximately correct the velocity field to make it divergence free.

In all simulations with AMR-Wind, both the Coriolis forcing and Boussinesq buoyancy model were included to capture the effects of wind veer and atmospheric stratification. The subgrid-scale kinetic energy one-equation turbulence model was employed to close the large-eddy simulation (LES) equations. At the lower boundary, the sub-filter scale stresses are applied following the formulation of [18]. A temperature inversion was also applied at z = 1500 m to limit the growth of the ABL in the vertical direction.

The wind farm simulations performed in this study were carried out in a two-stage process. In the first stage, a precursor calculation was used to develop the correct ABL inflow boundary conditions. The precursor calculation used an ABL forcing scheme where a constructed pressure gradient was applied to ensure that the hub-height wind speed at z = 91 m matched the anemometer measurements, and horizontally periodic boundary conditions were used. To arrive at the correct shear and turbulence intensity characteristics, two wall model parameters were varied at the ground: the surface roughness z_0 and the applied temperature gradient at the ground. Once the appropriate ABL conditions were established, the second stage of the simulation used the precursor solution as the initial condition and the saved boundary data as the inflow conditions. These calculations included additional mesh refinement and turbine models to capture the full operation of the AWAKEN wind farms.
Two sets of simulations were carried out with AMR-Wind. The first simulated all wind farms in AWAKEN [6], and only the results for the King Plains wind farm are shown here. The background mesh resolution (level 0) was 20 m × 20 m20 m and was successively refined to achieve 2.5 m × 2.5 m × 2.5 m mesh resolution (level 3) surrounding the turbine rotor regions. For the simulations that included the turbine models, the total mesh size was 21.14B elements. Simulations were run on 6000 GPUs on the Summit high-performance computing system at Oak Ridge Leadership Computing Facility, and have used approximately 1 million GPU-hours to this point. The second set simulated only the 50 turbines in the eastern portion of King Plains.

2.2.3. Nalu-Wind

The multiphysics, massively parallel code Nalu-Wind [2, 3] performs LES of the ABL, using a node-centered finite volume discretization to solve the acoustically incompressible Navier-Stokes equations with an approximate pressure projection technique, and a one equation, constant coefficient, turbulent kinetic energy model for the subgrid-scale stresses [19]. A wall function based on Monin-Obukhov theory is used for the bottom boundary, and an inflow/outflow boundary condition is used at the top [20]. The inflow/outflow condition uses a potential flow solution in wavenumber space which dampens high-frequency disturbances at the upper boundary. The boundary condition on the domain sides was periodic. The flow solver was coupled to an appropriate OpenFAST model for each turbine (https://nwtc.nrel.gov/OpenFAST).

ABL forcing source terms are provided to the momentum equation to drive the flow to a predetermined velocity at a specific height, where the force is proportional to the difference between the desired spatial averaged velocity and the horizontally averaged instantaneous velocity. Similar to AMR-Wind, a two-stage process was carried out, using a precursor calculation to develop the correct inflow boundary conditions and then a turbine calculation that uses the precursor solution data for both the initial flow field and inflow conditions. The wall model parameters of surface roughness z_0 and the surface heat flux at the ground were also calibrated to arrive at the correct shear and turbulence intensity characteristics. Coriolis forces were also taken into account. Unstable and stable ABL simulations using Nalu-Wind were performed for the King Plains wind farm. A 9.5 km × 9.5 km × 0.8 km domain was used for the stable ABL case and a 20 km × 20 km × 2.5 km domain was used for the unstable ABL case. The background mesh resolution was 20 m and 10 m for the unstable and stable cases, respectively, and were successively refined to achieve 2.5 m mesh resolution around the individual turbines. The total mesh sizes for the unstable and stable cases were 258 million and 245 million elements, respectively. The unstable and stable ABL cases simulated 41 and 31 turbines respectively, as the stable case did not incorporate a back row of ten turbines in King Plains that was simulated in the unstable case.

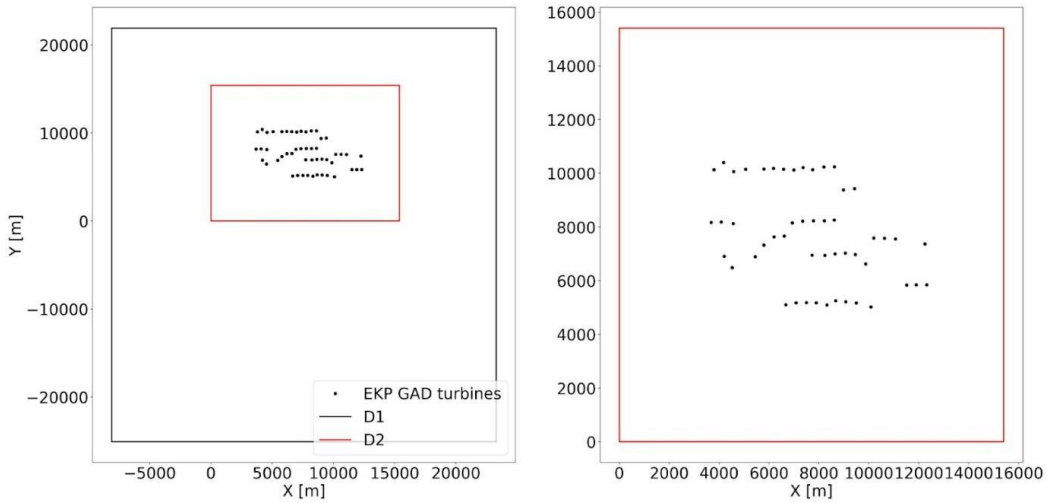

Fig. 2. Computational domains employed in the idealized WRF-LES-GAD simulations for eastern King Plains consist of a parent (D1) and a nest (D2), whereby the GAD is represented only in the nest. The origin of the local coordinate system is the southwest corner of the D2 domain. A fifty-turbine subset of King Plains was selected for the simulations, similar to one of the AMR-Wind setups.

2.2.4. WRF-LES-GAD

The multi-scale simulations were performed with the Advanced-Research Weather Research and Forecasting (WRF) model version 4.1.5 [4], which solves the compressible Euler equations for the three spatial dimensions and time. Several processes are included via parameterization schemes, such as for cloud formation physics, radiation, and the exchange of momentum, heat, and moisture with the land surface. The model is capable of running real forecasts for a selected region of the globe by using initial and boundary conditions derived from forecast systems or reanalysis products, such as ERA5. It can also run idealized simulations that are initialized with a user-specified dictionary containing vertical profiles of wind speed components, potential temperature, and moisture. In this paper, idealized simulations initialized by these user-specified profiles were employed.

Two computational domains were used for the idealized simulations (Fig. 2). The parent domain (D1) that uses periodic lateral boundary conditions and a nest domain (D2) with lateral boundary conditions specified and mapped from its parent. Both domains rely on WRF's large-eddy simulation (LES) capabilities and do not use planetary boundary layer (PBL) schemes. Thus, fine spatial resolutions of 100 m and 10 m were used. The D1 domain initializes with a constant wind speed of 14 m/s and direction of 190°based on trial and error. To reduce computational cost, the lower-resolution and cheaper domain D1 runs for 4 hours with the nest switched off to properly initialize turbulence and the desired boundary layer characteristics, in a fashion similar to that described in Idealized WRF. After 4 hr of spin-up time, the convective boundary layer and turbulence fully develop and reach an average hub-height wind speed of 9.4 − 9.6 m⁄s and a wind direction of about 170°. This will lead to higher power production. After the D1 is spun-up, the D2 domain is switched on and the wind farm simulation takes place from about 50 minutes.

The sensible heat flux (52 W⁄m^2) and surface roughness (0.15 m) are matched to the AMR-Wind setup. To accelerate the development of fine-scale turbulence in the nest, the cell-perturbation method (CPM), which applies random perturbations to the potential temperature field, was employed across the boundary layer [21]. Several physical processes and their associated parameterizations have been omitted from the simulations, such as moisture phase changes, cloud formation, and radiation. The Deardorff 1.5 TKE subgrid-scale model was used for the LES [22] with the nonlinear backscatter and anisotropy (NBA) model [23]. Four runs were performed in total: eastern King Plains with (case 1) and without turbines (case 2) considering a flat terrain, and eastern King Plains with (case 3) and without turbines (case 4) considering SRTM's 1/3 arc sec (~10 m) terrain elevation map within the innermost domain. The terrain was included in cases 3 and 4 only for the innermost D2 domain. The outermost domain D1 remained flat. The runs without turbines serve to isolate the turbine effects in the flow field.

2.3. Turbine representation

To lower the computational expense of the LES and to keep the models consistent between different

simulations types, all studies for this milestone used actuator disk models (ADM) to represent the turbine dynamics. An OpenFAST model that emulates the GE 2.8-127 turbine model used in King Plains by scaling publicly available reference turbines was developed [24]. The scaled model was tuned to match the correct hub height, rotor size, and power rating with reasonable approximations of the thrust behavior. No proprietary wind plant or turbine data were used in the simulations. The scaled models were tuned to match the correct hub height, rotor size, and power rating with reasonable approximations of the thrust behavior. The power and thrust curves are shown in Fig. 3.

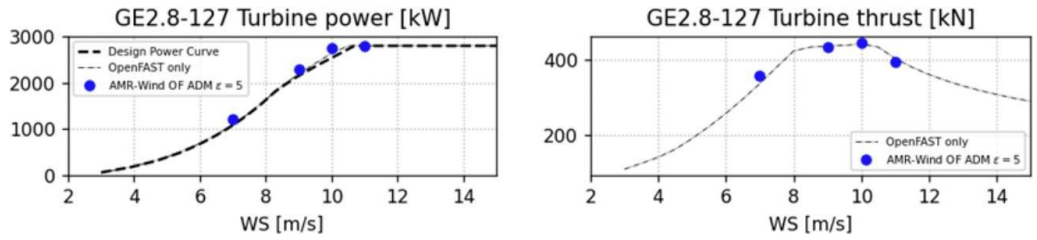

Fig. 3. Power and thrust curves for two of the turbines used in the simulations with OpenFAST models.

For the AMR-Wind and Nalu-Wind calculations, the actuator disc model parameterization also underwent a calibration process to accurately match the target power and thrust behavior. The calibration simulations were run in AMR-Wind on a smaller domain with a single turbine, represented using the ADM-Joukowski or ADM-OpenFAST model, placed in the center; three levels of mesh refinement were used to match the primary multi-farm simulations. As shown in Fig. 3, the power and thrust predictions from the calibration simulations were compared with the design curves of the respective turbines. Parameters such as the size of the isotropic smoothing kernel and the vortex core size in the Joukowski model were adjusted until the agreement was satisfactory for the wind speeds of interest. In the Nalu-Wind simulations, the ADM-OpenFAST coupled model was used for the GE 2.8-127 turbine. AMR-Wind calculations also used the ADM-OpenFAST coupled model for the GE 2.8-127 turbines at the King Plains wind farm.

Wind turbines were represented as generalized actuator disks (GAD) and implemented in the WRF code [25]. The current GAD implementation has a simple control mechanism that yaws the turbine toward the incoming wind direction. The GAD computes the raw aerodynamic power, which differs from the electric output of the real turbines. Thus, we have converted this raw aerodynamic power into output electric power by considering an efficiency of 90% and by limiting maximum power to the rated value (2.8 MW). An air density of 1.17 kg/m^3 was adopted.

3. RESULTS

3.1. Inflow conditions

A comparison of the horizontal velocity profiles at King Plains for the AMR-Wind, Nalu-Wind, and WRF-LES- GAD simulations shows the differences in the inflow velocities for the various solvers (Fig. 4). For the unstable ABL condition, the averaged horizontal velocity inflow was computed at approximately 30*D* and 19*D* upstream of the first row turbines in the AMR-Wind and Nalu-Wind simulations, respectively. For the WRF-LES-GAD simulations, the inflow profile was taken at the first turbine row (0.0*D* upstream) itself. Both the AMR-Wind and Nalu-Wind profiles agree well, and match the desired hub-height inflow velocity (9 m/s) and also show similar shear across the rotor disk. However, for the WRF simulations, the inflow hub-height wind was larger, approximately 9.4 m/s for the flat case, leading to higher power predictions.

In the stable ABL case, both the AMR-Wind and Nalu-Wind inflow profiles agree well near the ground and at hub-height. However, note that a lower inversion height was used for the stable case in AMR-Wind compared to Nalu-Wind to help accelerate the convergence time of the larger domain. This led to some differences in the inflow velocity profiles above hub-height, although the shear profile still agreed reasonably well.

3.2. Hub-height wind speed maps

Hub-height contours of horizontal velocity are used to allow a qualitative comparison between the simulated flow fields. In each case both an instantaneous and an averaged contour is shown. For the unstable ABL condition shown in Figs. 5 and 6, several immediate differences are apparent. Note that in the FLORIS Gaussian-Curl Hybrid model, the formulation is for a steady-state wake behavior, so the instantaneous and averaged velocity fields are identical. In the simulations where the large scale convective structures were

resolved (AMR-Wind, Nalu-Wind, and WRF simulations), the local variations in wind speed and direction are visible in both the instantaneous and the mean velocity fields. These convective structures lead to different inflow velocities for different turbines within the same wind farm, as well as differences in the wake propagation direction. Variations in the local yaw angle were accounted for in the AMR-Wind simulations, but all turbines in the Nalu-Wind simulation had a constant yaw heading of 175°, so yaw misalignment may be present. In the FLORIS model, both the wind speed and direction were constant everywhere, so each turbine is perfectly aligned with the flow.

For the stable ABL simulations (Fig. 7), the dominant length scales of the turbulent structures are much smaller than for the unstable case, and the resulting velocity fields are much more homogeneous. This leads to much smaller variations in wind speed across the turbines at the King Plains wind farm, and nearly uniform wind direc- tions and wake propagation directions for all turbines.

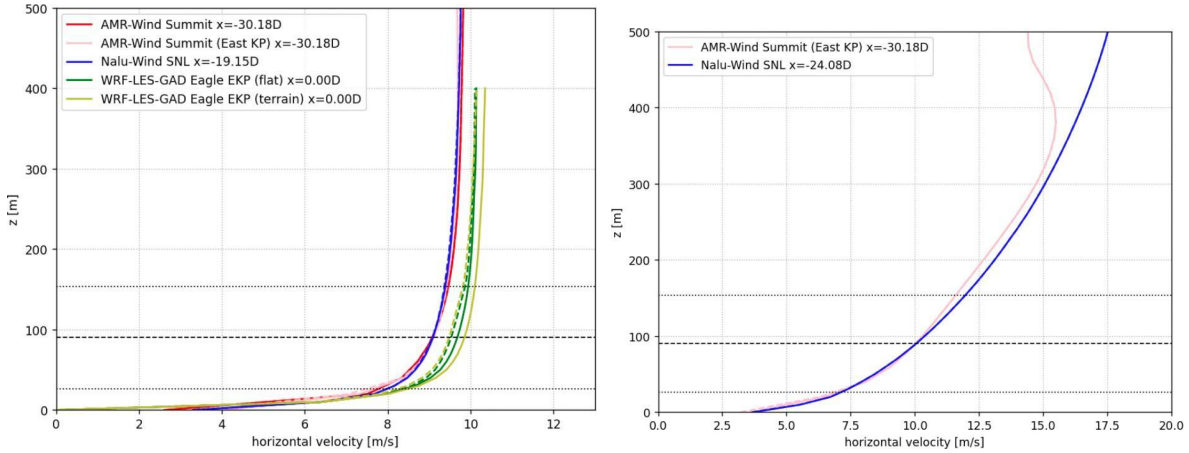

Fig. 4. Horizontal velocity profile for incoming wind for the unstable ABL (left) and the stable ABL (right) upstream of King Plains. Solid lines show precursor runs while dashed lines show runs that include turbines. The black dashed and dotted lines represent the turbine hub-height and rotor disk extents, respectively.

3.3. Wake effects

A more quantitative view of the wake behaviors can be seen by examining the averaged turbine centerline velocities for the turbines at King Plains. From each of the simulation models — FLORIS GCH, AMR-Wind, Nalu-Wind, and WRF — the centerline locations on the hub-height plane (following the local wind direction) can be extracted along with the averaged velocity components. A comparison of the normalized wake velocity on the centerline axis are shown for the unstable (Fig. 8, left) and stable (Fig. 8, right) cases.

The wake deficits for the WRF-LES-GAD model, both with and without terrain, showed the fastest recovery, followed by the FLORIS GCH model. The microscale LES simulations, Nalu-Wind and AMR-Wind, had the most persistent wakes, with AMR-Wind's wakes being the longest. For the stable ABL case, as expected, the wake recovery was slower compared to the unstable ABL case. The wakes predicted by Nalu-Wind were the most persistent in this set of simulations.

3.4. Flow-field inhomogeneity effects

Some additional insight can be gained by examining the wake centerline behavior for just the front row turbines of King Plains. For the unstable ABL case in Fig. 9, the differences between the AMR-Wind and Nalu-Wind wakes are still visible. However, we can relate these differences to some variations in the local ambient wind field as well as the ADM turbine models in the codes themselves. As mentioned before, the precursor horizontal velocity in Nalu-Wind at the front row turbines (x/D =0) is noticeably larger compared to AMR-Wind: approximately 9.3 m/s compared to 9.05 m/s for the large scale AMR-Wind calculation. However, there are differences in the observed vertical velocity at the centerline as well. Both the Nalu-Wind and the AMR-Wind (Eastern KP) simulations show a slightly negative vertical velocity, while the large-scale AMR-Wind simulation shows a stronger positive vertical velocity on the centerline. This suggests that the large-scale atmospheric structures may impart a downward or upward motion to the wakes depending on the simulation. Also worth noting is that the ADM implementation in Nalu-Wind neglects the turbine swirl component, so the wakes for AMR-Wind may include more upward motion (Fig. 9, bottom right).

Similar comparisons for the stable ABL case are shown in Fig. 10. A small difference in the horizontal velocities at front row turbines is also visible, accounting for some power differences. Under stable atmospheric stratification, the precursor velocity field has a negligible vertical velocity component, although the downstream

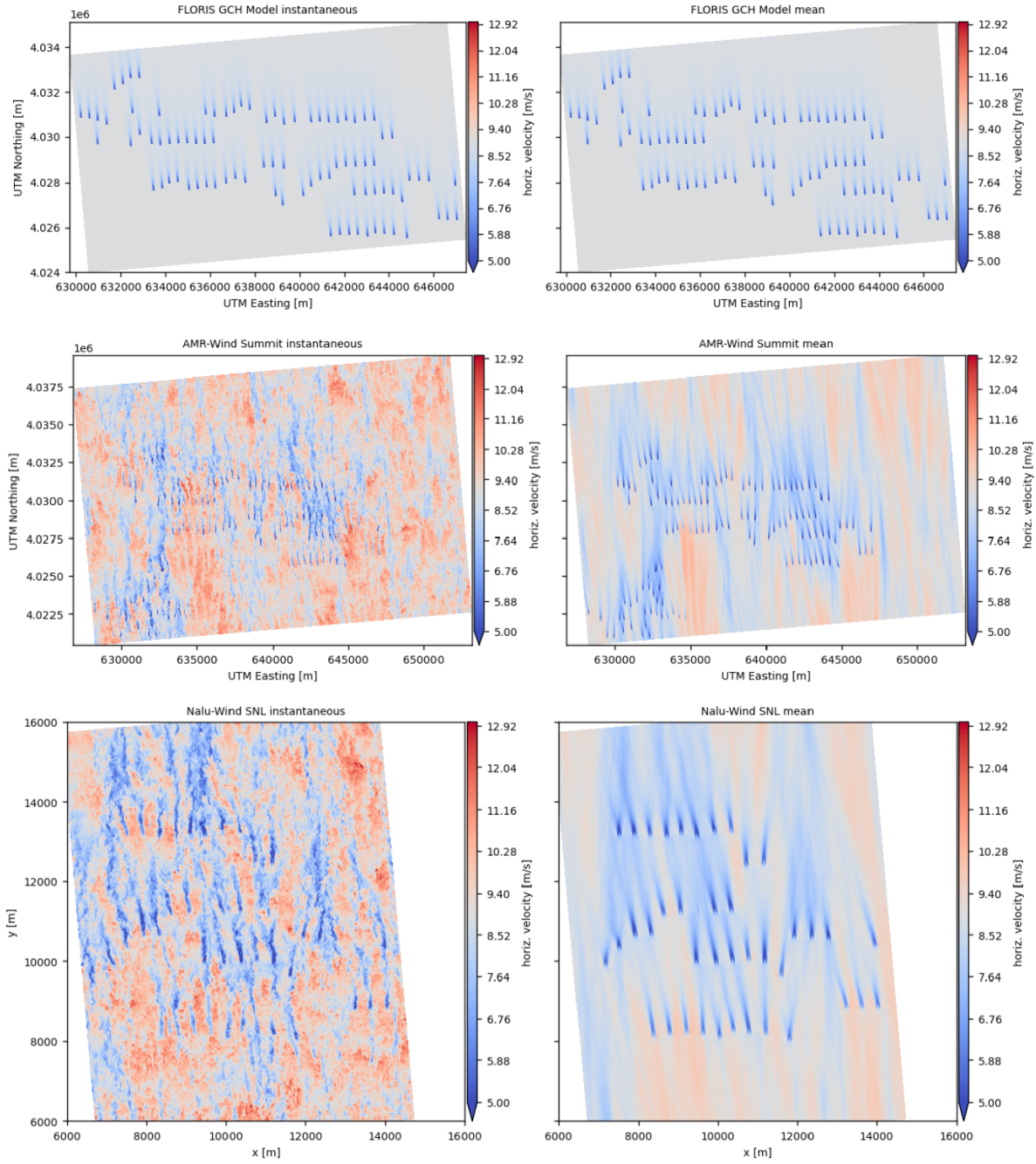

Fig. 5. Instantaneous (left) and mean (right) hub height planes for the King Plains wind plant with an unstable ABL for the various solvers (solver identities are annotated as the subplot titles).

wake still has varying degrees of vertical motion due to the differences in ADM implementation between the AMR-Wind and Nalu-Wind codes.

However, because the centerline locations were all extracted along a constant hub-height elevation, any vertical motion in the wake would not be accounted for, and the maximum wake deficit may not be captured in these centerline plots. In future analysis, rotor averaged velocities or wake-following coordinates should be used to more accurately capture the wake behavior.

3.5. Terrain effects

Fig. 11 shows the average ratio between hub-height wind speeds using WRF-LES-GAD for the convective case of the terrain case to the flat case ($SU = WS_{terrain}/WS_{flat}$) for both the no-turbine (left) and the turbine (right)

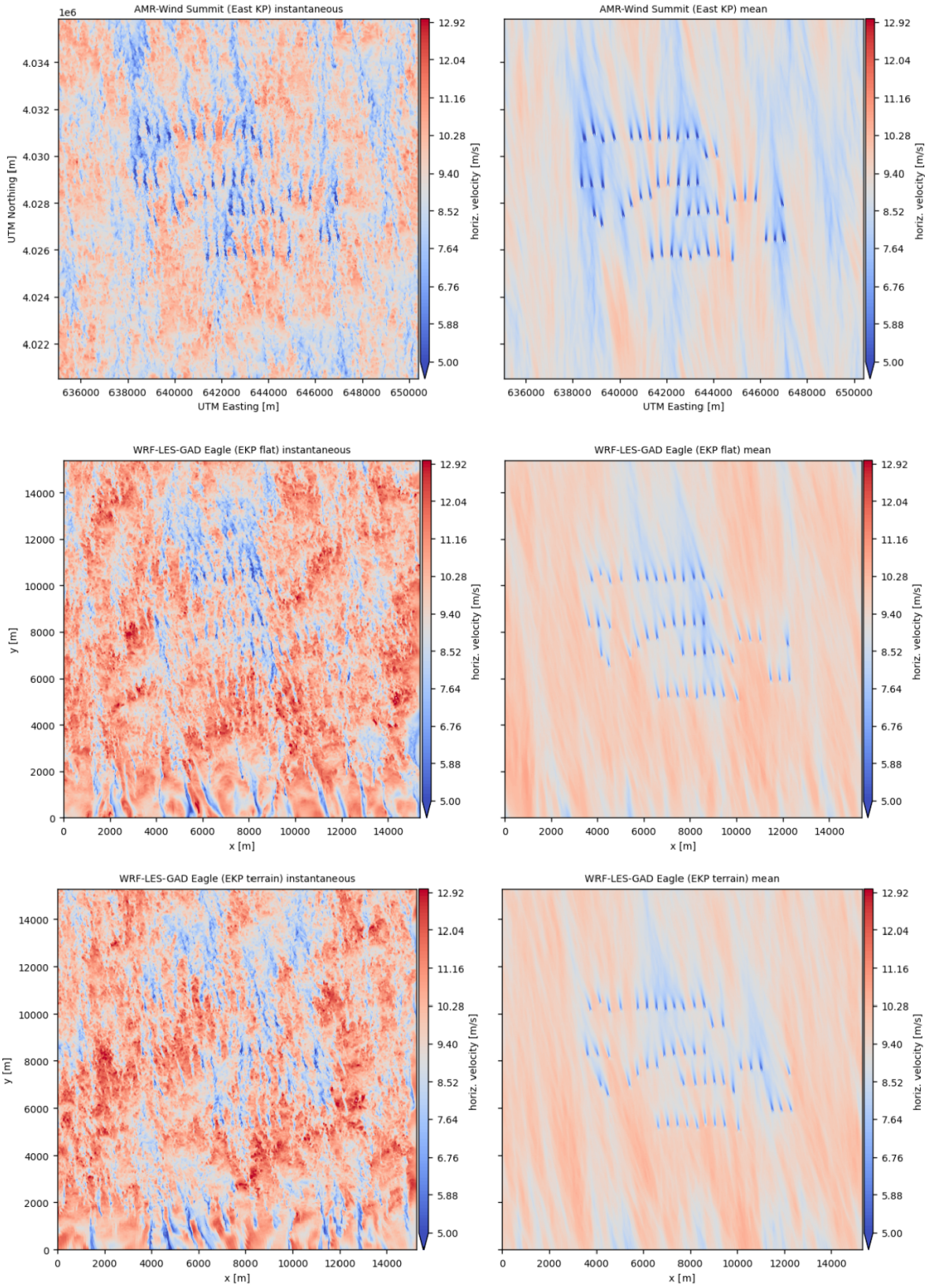

Fig. 6. Continuation of Fig. 5.

situation to better illustrate and isolate the topographic effects on the flow field.

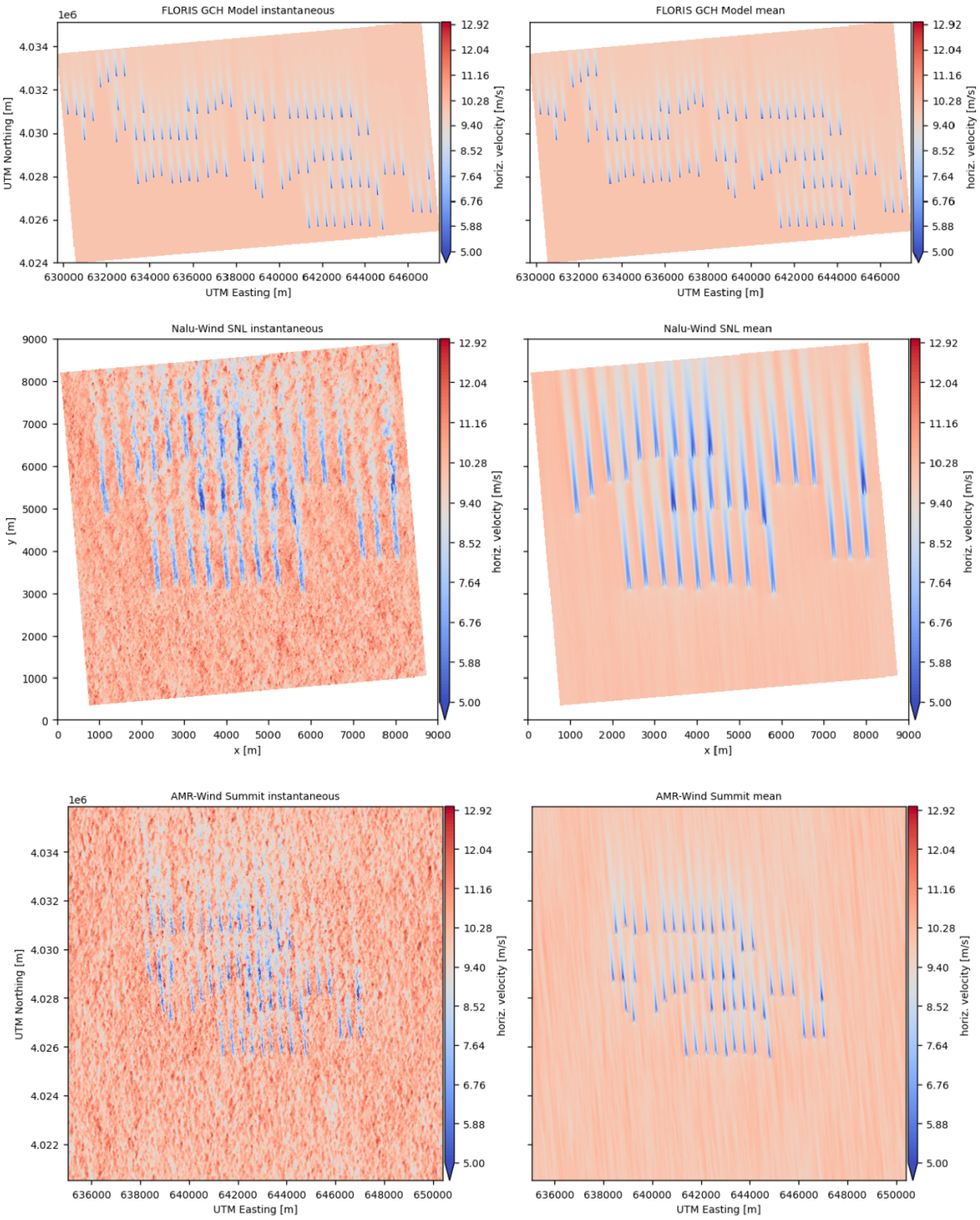

Fig. 7. Instantaneous (left) and mean (right) hub height planes for the King Plains wind plant with a stable ABL for the various solvers (solver identities are annotated as the subplot titles).

Two distinctive areas are discernible in the speed-up (*SU*) map: some patches of wind acceleration (colored red, *SU* > 1.1) elongated in the along-wind direction are located near the higher ground in the central and western portions of KP. Acceleration is maximum immediately west of the wind farm in an area without turbines in the plot – the real KP wind farm, however, does have turbines operating in that location. The eastern portion of KP is crossed by an area of relatively lower speeds (*SU* < 0.9) that extends from the domain inlet toward the outlet in the along-wind direction. Turbines in this region will experience lower wind speeds. Despite the absence of site-specific measurements to compare against yet, the topographic acceleration over higher ground and deceleration near lower ground is a well-known feature of wind flow over topography in convection conditions.

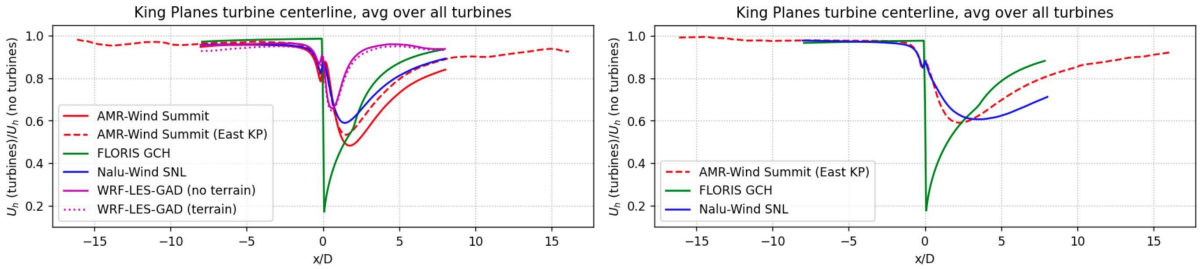

Fig. 8. The wake deficit measured along the centerline and averaged for all the turbines in each simulation for unstable (left) and stable (right) conditions.

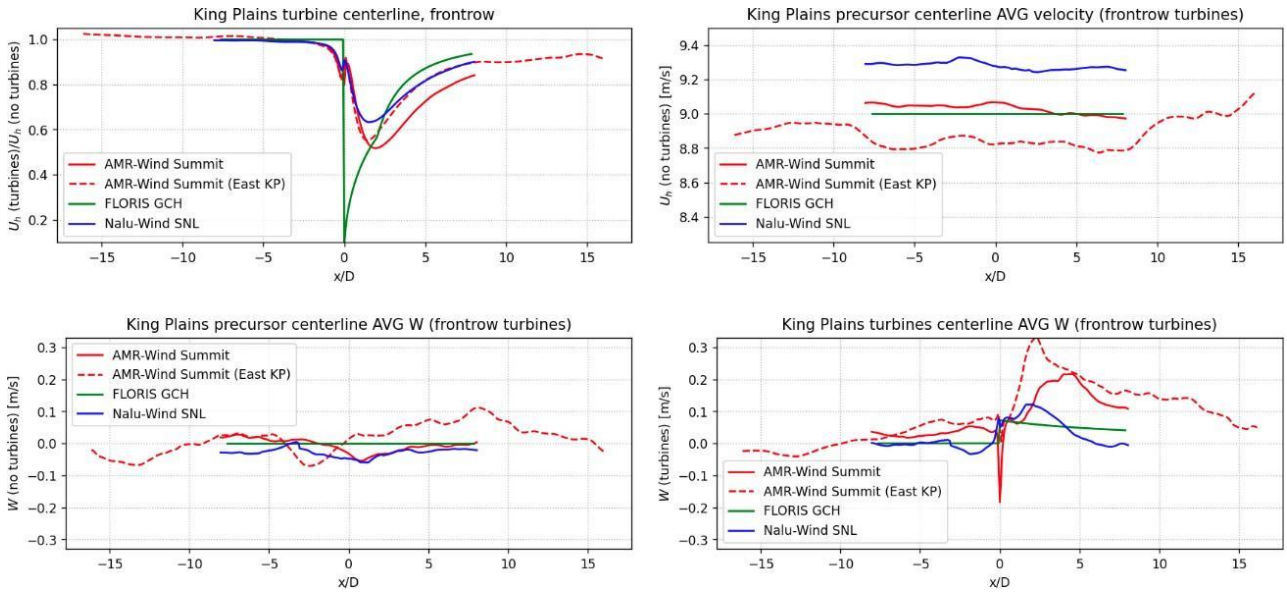

Fig. 9. The wake deficit measured along the centerline and averaged for the front row of turbines in each simulation for the unstable ABL condition. The top row shows the horizontal velocity and the bottom row shows the vertical velocity. A comparison of the wind along the same centerline but without the turbines (AMR-Wind Summit (East KP)) is also shown.

No simulations have been carried out for the stable case, but the scientific literature on stratified flows over topography indicates that there would be flow field acceleration and deceleration different in character from the convective case. In stable conditions, in the absence of turbines, winds are likely to accelerate descending the slopes and to decelerate ascending the slopes, so that the speed-up map would be different.

The presence of the wind turbines will interact non-linearly with the topographic speed-up field producing a large spatial variability in the wake field (Fig. 11, right). The area of reduced wind speeds in the eastern portion of KP for the no-turbine case interacts with the eastern turbines producing stronger and longer wakes, identifiable as a blue patch stretched in the along-wind direction. In other parts of the wind farm there is spatial heterogeneity and turbines experience either weaker or stronger wakes because of the topographic effects. Interestingly, it seems that the presence of the wind farm alleviates the spatial variability in the flow field around it and downstream. This is because the formerly strongly red and blue areas for the no-turbine cases (Fig. 11, left) have been broken down into smaller and weaker patches of either weaker or stronger wind speeds (Fig. 11, right).

4. CONCLUSIONS

In this paper, results from a model intercomparison benchmark aimed at simulating the King Plains wind farm in idealized unstable and stable conditions were presented. The LES-based models AMR-Wind, Nalu-Wind and WRF-LES-GAD were compared with the engineering model FLORIS. The main goal was to assess the influence of features such as ADM implementation, terrain, stability and other model-specific setups on the

simulated wind, turbulence, wakes and performance.

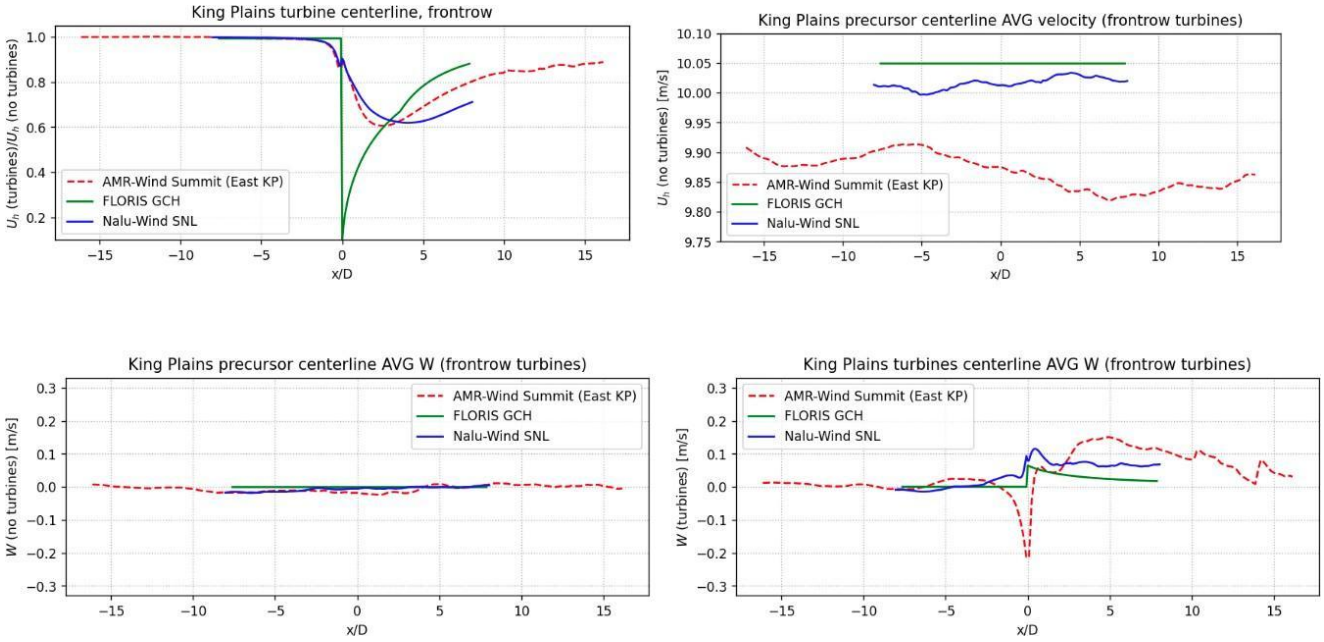

Fig. 10. The wake deficit measured along the centerline and averaged for the front row of turbines in each simulation for the stable ABL condition. The top row shows the horizontal velocity and the bottom row shows the vertical velocity. A comparison of the wind along the same centerline but without the turbines (AMR-Wind Summit (East KP)) is also shown.

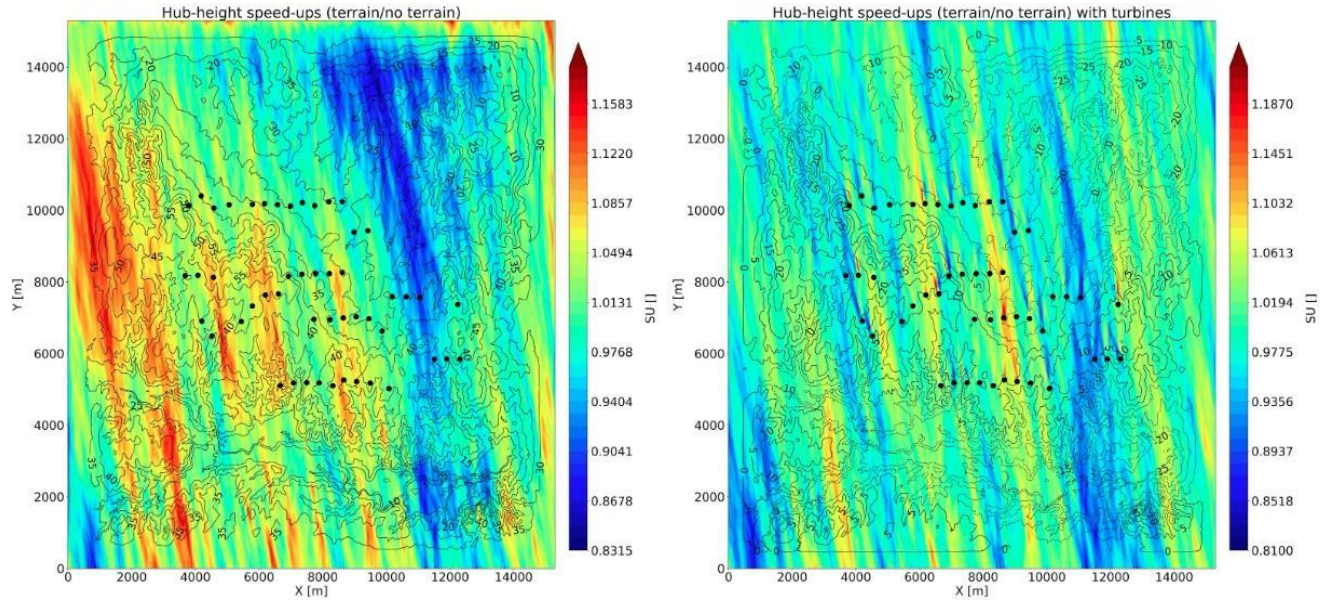

Fig. 11. Average hub-height speed-ups obtained as the ratio between the terrain and no terrain cases without turbines (left) and with turbines (right) using WRF-LES-GAD for the convective cases for eastern King Plains (EKP). Wind farm layout is overlaid to highlight which turbine clusters are affected by the spatial variability in the flow field caused by the topography. Terrain contour levels are colored black and some heights are displayed. Terrain elevation was normalized so that the minimum level in the plot is 0 m. The central and western turbines closer to higher ground will benefit from wind acceleration (red areas), whereas those in the eastern side will suffer wind deceleration (blue areas). Despite the mild changes in elevation, these seem sufficient to produce noticeable changes in speed-up. Wake dynamics and turbine performance will be influenced.

Regarding the flow field, turbulent structures in unstable conditions produce stronger spatial variability than stable conditions, which leads to variability in power production among unwaked turbines, even in flat

terrain. Conversely, in stable conditions the length scale of turbulent structures is much smaller, which produces less patial variability in the flow field, power production of unwaked turbines, yaw and wake propagation direction. FLORIS being an engineering model assumes a homogeneous inflow and does not represent flow field variability in both unstable and stable cases.

Wakes in unstable conditions are shorter in the streamwise direction and spread faster in the cross-wind direction because of the enhanced momentum entrainment. On the other hand, in stable conditions wakes are longer and thinner because of the weaker momentum entrainment. Differences in wake characteristics across models can be attributed to slight differences in the inflow and the flow field variability (especially in unstable conditions), ADM implementation and yawing capability, in general. In the case of WRF-LES-GAD in unstable conditions, in addition to the stronger inflow speed and turbulence, a GAD method shortcoming at wind speeds near rated may have contributed to the much shorter wake. Other differences in the ADM implementation, such as that Nalu-Wind neglects the turbine swirl component, may cause less wake upward motion near the rotor. Finally, the certerline velocity deficit may not be the most appropriate wake metric, since the wakes are transported vertically by updrafts and downdrafts of air; a rotor-averaged deficit could be a better option.

The presence of topography produces a notable influence in the spatio-temporal variability of the flow and wake fields during convective conditions. This effect causes some clusters of turbines to either under-perform or outperform, and to produce either shorter and weaker or longer and stronger wakes in comparison with the flat case. The interaction between the topographic speed-up and the turbines seem to break down the flow and turbulence field into smaller patches with heterogeneous speed-ups. Stable conditions have not been simulated with the terrain, but there is likely to be flow acceleration down the slopes and deceleration up the slopes, thus producing a different speed-up field. On top of that, the role of stable wakes, blockage, and gravity waves should be considered in the future.

ACKNOWLEDGEMENTS

This research was supported by the Wind Energy Technologies Office of the U.S. Department of Energy (DOE) Office of Energy Efficiency and Renewable Energy. Sandia National Laboratories is a multi-mission laboratory managed and operated by National Technology & Engineering Solutions of Sandia, LLC (NTESS), a wholly owned subsidiary of Honeywell International Inc., for the U.S. Department of Energy's National Nuclear Security Administration (DOE/NNSA) under contract DE-NA0003525. This written work is authored by an employee of NTESS. The employee, not NTESS, owns the right, title and interest in and to the written work and is responsible for its contents. Any subjective views or opinions that might be expressed in the written work do not necessarily represent the views of the U.S. Government. The publisher acknowledges that the U.S. Government retains a non-exclusive, paid-up, irrevocable, world-wide license to publish or reproduce the published form of this written work or allow others to do so, for U.S. Government purposes. The DOE will provide public access to results of federally sponsored research in accordance with the DOE Public Access Plan. This research used computational resources of the Oak Ridge Leadership Computing Facility at the Oak Ridge National Laboratory, which is supported by the Office of Science of the U.S. DOE under Contract No. DE-AC05-00OR22725; and was also sponsored by the DOE's Office of Energy Efficiency and Renewable Energy located at the National Renewable Energy Laboratory. W. Radünz would like to thank FAPESP, grant number 2022/04474-6, for financial support. B. Carmo and P. Peixoto thank the CNPq for financial support in the form of a productivity grants, respectively numbers 314221/2021-2 and 303436/2022-0. P. Peixoto would like to thank FAPESP, grant number 2021/06176-0, for financial support.

References

[1] P. M. O. Gebraad, F. W. Teeuwisse, J. W. van Wingerden, P. A. Fleming, S. D. Ruben, J. R. Marden, L. Y. Pao, Wind plant power optimization through yaw control using a parametric model for wake effects - a CFD simulation study, Wind Energy 19 (1) (2016) 95–114. doi:10.1002/we.1822.

[2] M. A. Sprague, S. Ananthan, G. Vijayakumar, M. Robinson, ExaWind: A multifidelity modeling and simulation environment for wind energy, Journal of Physics: Conference Series 1452 (1) (2020) 012071. doi:10.1088/ 1742-6596/1452/1/012071.

[3] S. P. Domino, "Sierra Low Mach Module: Nalu Theory Manual 1.0" Sandia National Laboratories Unclassified Unlimited Release (UUR) In: SAND2015-3107W (2015).
URL https://github.com/NaluCFD/NaluDoc

[4] W. C. Skamarock, J. B. Klemp, J. Dudhi, D. O. Gill, D. M. Barker, M. G. Duda, X.-Y. Huang, W. Wang, J. G. Powers, A Description of the Advanced Research WRF Version 4, Technical Report (2019) 113doi: 10.5065/D6DZ069T.

[5] H. Asmuth, H. Korb, S. Ivanell, How Fast is Fast Enough? Industry Perspectives on the Use of Large-eddy Simulation in Wind Energy, Journal of Physics: Conference Series 2505 (1) (2023) 012001. doi:10.1088/1742-6596/2505/1/012001.

[6] L. Cheung, A. Hsieh, M. Blaylock, T. Herges, N. DeVelder, K. Brown, P. Sakievich, et al., Investigations of Farm-to-Farm Interactions and Blockage Effects from AWAKEN Using Large-Scale Numerical Simulations, Journal of Physics: Conference Series 2505 (1) (2023) 012023. doi:10.1088/1742-6596/2505/1/012023.

[7] M. Sanchez Gomez, J. K. Lundquist, J. D. Mirocha, R. S. Arthur, D. Mun˜oz-Esparza, R. Robey, Can lidars assess wind plant blockage in simple terrain? A WRF-LES study, Journal of Renewable and Sustainable Energy 14 (6) (2022) 063303. doi:10.1063/5.0103668.

[8] P. A. Taylor, H. W. Teunissen, The askervein hill project: overview and background data, Boundary-Layer Meteorology 39 (1987) 15–39. doi:10.1007/s10546-011-9637-x.

[9] A. Bechmann, J. Berg, M. Courtney, H. Ejsing Jørgensen, J. Mann, N. N. Sørensen, The Bolund experiment: overview and background (2009).

[10] J. M. Wilczak, M. Stoelinga, L. K. Berg, J. Sharp, C. Draxl, K. Mccaffrey, R. M. Banta, L. Bianco, et al., The Second Wind Forecast Improvement Project (WFIP2): Observational Field Campaign, Bulletin of the American Meteorological Society 5 (2019) 1–60. doi:10.1175/BAMS-D-18-0035.1.

[11] H. J. S. Fernando, J. Mann, J. M. L. M. Palma, J. K. Lundquist, R. J. Barthelmie, M. Belo-Pereira, W. O. J. Brown, F. K. Chow, et al., The Perdiga˜o: Peering into Microscale Details of Mountain Winds, Bulletin of the American Meteorological Society 100 (5) (2019) 799–819. doi:10.1175/BAMS-D-17-0227.1.

[12] M. Debnath, A. K. Scholbrock, D. Zalkind, P. Moriarty, E. Simley, N. Hamilton, C. Ivanov, et al., Design of the American Wake Experiment (AWAKEN) field campaign, Journal of Physics: Conference Series 2265 (2) (2022) 022058. doi:10.1088/1742-6596/2265/2/022058.

[13] N. G. Nygaard, S. T. Steen, L. Poulsen, J. G. Pedersen, Modelling cluster wakes and wind farm blockage, Journal of Physics: Conference Series 1618 (6) (2020) 062072. doi:10.1088/1742-6596/1618/6/062072.

[14] A. Niayifar, F. Porte´-Agel, Analytical Modeling of Wind Farms: A New Approach for Power Prediction, Energies 9 (9) (2016) 741. doi:10.3390/en9090741.

[15] A. S. Almgren, J. B. Bell, P. Colella, L. H. Howell, M. L. Welcome, A Conservative Adaptive Projection Method for the Variable Density Incompressible Navier–Stokes Equations, Journal of Computational Physics 142 (1) (1998) 1–46. doi:10.1006/jcph.1998.5890.

[16] K. Sverdrup, N. Nikiforakis, A. Almgren, Highly parallelisable simulations of time-dependent viscoplastic fluid flow with structured adaptive mesh refinement, Physics of Fluids 30 (9) (2018) 093102. doi:10.1063/1.5049202.

[17] E. Motheau, J. Wakefield, Investigation of finite-volume methods to capture shocks and turbulence spectra in compressible flows, Communications in Applied Mathematics and Computational Science 15 (1) (2020) 1–36. doi:10.2140/camcos.2020.15.1_.

[18] C.-H. Moeng, A Large-Eddy-Simulation Model for the Study of Planetary Boundary-Layer Turbulence, Journal of the Atmospheric Sciences 41 (13) (1984) 2052–2062. doi:10.1175/1520-0469(1984)041<2052:ALESMF> 2.0.CO;2.

[19] A. Yoshizawa, K. Horiuti, A Statistically-Derived Subgrid-Scale Kinetic Energy Model for the Large-Eddy Simulation of Turbulent Flows, Journal of the Physical Society of Japan 54 (8) (1985) 2834–2839. doi:10.1143/JPSJ.54.2834.

[20] R. Vasaturo, I. Kalkman, B. Blocken, P. van Wesemael, Large eddy simulation of the neutral atmospheric boundary layer: performance evaluation of three inflow methods for terrains with different roughness, Journal of Wind Engineering and Industrial Aerodynamics 173 (2018) 241–261. doi:10.1016/j.jweia.2017.11.025.

[21] D. Muñoz-Esparza, B. Kosovic, J. van Beeck, J. Mirocha, A stochastic perturbation method to generate inflow turbulence in large-eddy simulation models: Application to neutrally stratified atmospheric boundary layers, Physics of Fluids 27 (3). doi:10.1063/1.4913572.

[22] J. W. Deardorff, Stratocumulus-capped mixed layers derived from a three-dimensional model, Boundary-Layer Meteorology 18 (4) (1980) 495–527. doi:10.1007/BF00119502.

[23] B. Kosovic, Subgrid-scale modelling for the large-eddy simulation of high-Reynolds-number boundary layers, Journal of Fluid Mechanics 336 (1997) 151–182. doi:10.1017/S0022112096004697.

[24] E. Quon, NREL 2.8MW to OpenFAST 3.1.0 (2022).
URL https://github.com/NREL/openfast-turbine-models/tree/master/IEA-scaled/NREL-2.8-127

[25] J. D. Mirocha, B. Kosovic, M. L. Aitken, J. K. Lundquist, Implementation of a generalized actuator disk wind turbine model into the weather research and forecasting model for large-eddy simulation applications, Journal of Renewable and Sustainable Energy 6 (1). doi:10.1063/1.4861061.